Please do not adjust margins

Journal Name

ARTICLE

AsymPol-TEKs as efficient polarizing agents for MAS-DNP in glass matrices of non-aqueous solvents

Received 00th January 20xx,
Accepted 00th January 20xx

DOI: 10.1039/x0xx00000x

www.rsc.org/

Rania Harrabi[a], Thomas Halbritter[b], Shadi Alarab[a], Satyaki Chatterjee[b], Malgorzata Wolska-Pietkiewicz[c], Krishna K. Damodaran[b], Johan van Tol[e], Daniel Lee[a,d], Subhradip Paul[a], Sabine Hediger[a], Snorri Th. Sigurdsson*[b], Frederic Mentink-Vigier*[e], Gaël De Paëpe*[a]

Two polarizing agents from the AsymPol family, AsymPol-TEK and cAsymPol-TEK (methyl-free version) are introduced for MAS-DNP applications in non-aqueous solvents. The performance of these new biradicals is rationalized in detail using a combination of Electron Paramagnetic Resonance spectroscopy, Density Functional Theory, Molecular Dynamics and quantitative MAS-DNP spin dynamics simulations. By slightly modifying the experimental protocol to keep the sample temperature low at insertion, we are able to obtain reproducable DNP-NMR data with 1,1,2,2-tetrachloroethane (TCE) at 100 K, which facilitates optimization and comparison of different polarizing agents. At intermediate magnetic fields, AsymPol-TEK and cAsymPol-TEK provide 1.5 to 3-fold improvement in sensitivity compared to TEKPol, one of the most widely used polarizing agents for organic solvents, with significantly shorter DNP build-up times of ~ 1 s and ~ 2 s at 9.4 and 14.1 T respectively. In the course of the work, we also isolated and characterized two diastereoisomers that can form during the synthesis of AsymPol-TEK; their difference in performance is described and discussed. Finally, the advantages of the AsymPol-TEKs are demonstrated by recording 2D ^{13}C-^{13}C correlation experiments at natural ^{13}C-abundance of proton-dense microcrystals and by polarizing the surface of ZnO nanocrystals (NCs) coated with diphenyl phosphate ligands. For those experiments, cAsymPol-TEK yielded a three-fold increase in sensitivity compared to TEKPol, corresponding to a nine-fold time saving.

Introduction

Magic Angle Spinning Dynamic Nuclear Polarization (MAS-DNP) has expanded the scope of solid-state Nuclear Magnetic Resonance (ssNMR) spectroscopy.[1–6] MAS-DNP boosts ^1H spin polarization by taking advantage of the higher polarization of unpaired electrons spins that are present in so-called Polarizing Agents (PAs).[7,8] This results in an improved sensitivity that enables applications to challenging materials and the study of complex biomolecular systems.[9–20]

Several DNP mechanisms have been reported at high magnetic fields, including the Solid Effect, the Overhauser Effect, and the Cross Effect.[2] The Cross-Effect (CE) is currently the most efficient in terms of sensitivity[3,21–24] and necessitates the use of PAs containing two coupled electron spins.[7] The electron spin polarization difference is transferred to the isotope of interest via a complex mechanism driven by the sample spinning and microwave (μw) irradiation[3,5,25–34] at cryogenic temperature (typically ~100 K[35,36] or lower[4,37–44]). However, further improvements remain mandatory to fully unlock the potential of MAS-DNP especially for challenging samples, and at high magnetic fields and fast MAS frequencies. This has triggered the continuous development of PAs for MAS-DNP, from the introduction of improved bis-nitroxides[45–49] to hetero-biradicals such as trityl-nitroxides[50–55] and BDPA-nitroxides.[56,57]

PAs are designed for use in either aqueous matrices or in organic solvents, depending on the systems studied. The use in organic solvents is critical for systems that are incompatible with water.[16,19,58] The development of PAs for organic solvents is thus vital for many applications, and the specific challenges associated with the use of these solvents must be overcome. A few PAs have been described for MAS-DNP applications in organic solvents. The bTbK family,[48,59–61] which includes TEKPol[48] (Figure 1) and NaphPol,[61] along with the heterobiradicals HyTEK-2[57] and PyrroTriPol-OMe[54] are so far the best PAs for MAS-DNP experiments in non-aqueous solvents. At intermediate fields (9.4 and 14.1 T), PAs based on bis-nitroxides are still a good option, owing to their relative hyperpolarization efficiency, more facile synthesis, and ease of tuning the performance by chemically-controlling the e-e couplings and the *g*-tensor relative orientation.[45,46,49] However, the bTbK family is less efficient at high magnetic field and fast MAS frequencies,[56] in part due to their relatively weak electron-electron (e-e) coupling.[27,28,34,48,62] The weak coupling is also responsible for a large depolarization effect[28,31,34] and a longer hyperpolarization build-up time.[28,34] To go beyond the

a. *Univ. Grenoble Alpes, CEA, CNRS, IRIG, MEM, 38000 Grenoble (France)*
b. *University of Iceland, Department of Chemistry, Science Institute, Dunhaga 3, 107 Reykjavik (Iceland)*
c. *Faculty of Chemistry, Warsaw University of Technology, Noakowskiego 3, 00-664 Warsaw (Poland)*
d. *Current address: Department of Chemical Engineering, University of Manchester, Manchester, M13 9PL, UK*
e. *National High Magnetic Field Laboratory, Florida State University, Tallahassee, FL 32301 (USA)*
Email: snorrisi@hi.is, fmentink@magnet.fsu.edu, gael.depaepe@cea.fr

Please do not adjust margins

performance of the bTbK family, it is necessary to make new biradicals with stronger e-e couplings that can quickly generate large nuclear hyperpolarization, even for samples with large proton concentration,[49] and/or under high spinning frequencies.[27,45,51] This strategy has previously been applied to the AsymPol radical family, which was shown to provide excellent DNP performance in aqueous solutions (AsymPol-POK and cAsymPol-POK)[45,49] due to a sizable e-e coupling and a near orthogonal relative orientation of the two nitroxides.[28,29]

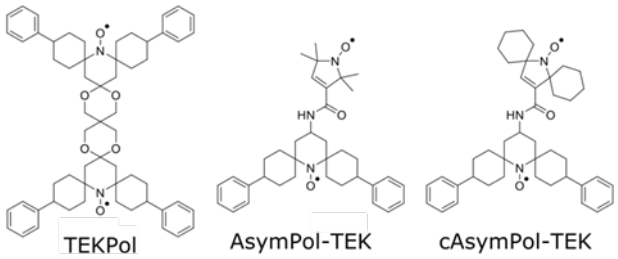

Figure 1 Structures of TEKPol, AsymPol-TEK, and cAsymPol-TEK.

Here we describe the synthesis and characterization of two new members of the AsymPol family, AsymPol-TEK and cAsymPol-TEK, for use in organic solvents. Interestingly, the synthesis yields two stereoisomers that do not provide the same DNP-NMR efficiency. Focusing on the better performing isomer, we show that AsymPol-TEK and cAsymPol-TEK have a higher DNP efficiency than TEKPol, thanks to their very fast build-up at both 9.4 and 14.1 T. Their performance is rationalized by a combination of DFT computations, Electron Paramagnetic Resonance (EPR) experiments, Molecular Dynamics simulations (MD) and a predictive numerical model.[49,30,33] In particular, DFT and multi-frequency EPR simulations enable estimating the electron dipolar coupling, the exchange interactions (*J*), the relative orientation of the *g*-tensors, and the ratio of the two main conformers.

For MAS-DNP applications, the solvent matrix must form a glass at cryogenic temperature to provide adequate spin relaxation properties and ensure a uniform distribution of the PAs.[4,63] In addition, the ^{1}H nuclei of the solvent must relax slowly. Only a handful of organic solvents have proven suitable for MAS-DNP experiments[58] and 1,1,2,2-tetrachloroethane (TCE), is currently one of the most used.[16,18,58,64–67] Nevertheless TCE remains challenging to use and several factors affect the DNP efficiency when using it.[58,68,69] It can form a glass phase at 100 K with rapid cooling of the sample, but crystalline phases can also be generated between 100 K and 200 K. Chlorinated solvent can dissolve a large amount of O_2 at room temperature (tens of mM)[70,71] which enhances the ^{1}H relaxation rate and lower the DNP efficiency. Degassing or packing of the sample under inert atmosphere is often used to overcome this problem.[66,68,72]

We thus addressed sample preparation, which is important for optimal DNP results. We confirmed that minimizing the oxygen content of the sample is important for TEKPol but less for the AsymPol-TEKs and demonstrate the critical importance to insert the sample into a probe sufficiently cold (~100 K or lower). The commonly used freeze-thaw cycle procedure[68] was modified to introduce the sample in absence of μw irradiation. Slightly higher probe temperatures, e.g. > 110 K, have a direct impact on the glass quality and DNP efficiency. This approach drastically improves the reproducibility of the DNP-NMR data and solves one of the problems associated with the use of TCE thus far. Finally, we illustrate the performance of the AsymPol-TEKs by reporting 2D ^{13}C-^{13}C correlation experiments at natural ^{13}C-abundance of proton-dense microcrystals and to hyperpolarize the surface of ZnO nanocrystals (NCs). For those experiments, cAsymPol-TEK yielded a three-fold increase in sensitivity compared to TEKPol, corresponding to a nine-fold time saving.

Material and methods

Sample preparation for MAS-DNP experiments. TEKPol was purchased from Cortecnet; AsymPol-TEK and cAsymPol-TEK (Figure 1) were synthesized as described below. 10±0.5 and 16±0.5 mM solutions of TEKPol, AsymPol-TEK and cAsymPol-TEK were prepared in fully protonated 1,1,2,2-tetrachloroethane (TCE). Hexagonal boron nitride (h-BN), adenosine and caffeine powders were purchased from Sigma-Aldrich and used as received without further purification. For the tests on the TCE solvent itself, 30 mg of h-BN was mixed with 30 μL of 10 or 16 mM TEKPol, AsymPol-TEK, cAsymPol-TEK in TCE. For the experiments on organic microcrystals, 30 mg of caffeine or adenosine powder were impregnated with 25 μL of 10 mM radical solution in TCE. The total weight of sample inside the rotor was estimated to be ∽25 mg, by weighing the rotor before and after the sample was packed. For the DNP experiments on the ZnO nanocrystals coated with monoanionic diphenyl phosphate (DPP) ligands, the ZnO NC powder was heated at a temperature of 90 °C for 14 h, and then subsequently impregnated with 10 mM cAsymPol-TEK in TCE, before being packed into a 3.2 sapphire rotor.

MAS-DNP experiments. Experiments were carried out at CEA-Grenoble (Grenoble, France) on a Bruker 9.4 T / 400 MHz (^{1}H frequency) / 263 GHz (electron frequency)[35] and at the National MagLab (Tallahassee, USA) on the 14.1 T / 600 MHz / 395 GHz MAS-DNP setup.[73] Both instruments are equipped with a Bruker Avance III console and a 3.2 mm wide-bore MAS-DNP probe capable of doing MAS NMR at 100 K. All samples were packed into 3.2 mm sapphire rotors and closed with Vespel caps. On the 600 MHz DNP setup, the μw power and the Martin-Puplett interferometer position were adapted to maximize the DNP

effect.[41,73] To characterize the MAS-DNP performance, the ^{13}C signal intensity of either the solvent TCE or the impregnated powders was measured through a ^{1}H-^{13}C CP experiment. Except if specified otherwise, a 100 kHz RF field was used for ^{1}H decoupling. A 1 to 2 ms ramped (80 to 100%) CP was used on the ^{1}H channel to match a Hartman-Hahn CP condition, with the ^{13}C RF field strength set to 50 kHz. The polarization build-up time T_B was obtained from proton saturation-recovery experiments under μw irradiation. The DNP enhancement factor $\varepsilon_{\mathrm{On/Off}}$, the depolarization factor $\varepsilon_{\mathrm{depo}}$ and the sensitivity were measured according to previous protocols.[49] Additional details can be found in the SI.

Modified freeze-thaw cycle procedure with TCE. To test the repeatability of the measurements on samples containing TCE, a freeze-thaw cycle was performed between each repeated experiment, using the following procedure. The rotor was ejected and kept either in the rotor catcher inside the probe base or on the bench. The μw irradiation was then turned off, while the bearing and drive pressures were raised to 800 mbar and the VT maintained to the same level as for the experiments. After 5 minutes, the rotor was inserted again in the cold probe head. We observed that keeping the μw off while inserting and spinning up the sample is critical to optimize the glass formation as it avoids heating the sample and generating crystalline phases.

Electron Paramagnetic Resonance (EPR) experiments. Continuous wave (CW) EPR measurements were carried out at 9.6 and 240 GHz electron resonance, both at a temperature of 100 K. At 9.6 GHz, samples were measured inside the sapphire rotor on an EMX-Nano using a N_2 cooled Dewar. The field modulation was set to 0.1 mT and the μw power to 1 μW to avoid signal saturation. The 240 GHz spectrum were measured under the same conditions as previously described.[33,49,54,74] The field modulation was set to 0.3 mT and the μw power was reduced in order to avoid signal saturation. The calibration of the magnetic field allows the determination of the *g*-values with a global uncertainty of 2×10^{-4}.[30,33,49]

MAS-DNP simulations. Simulations were performed with the latest implementation of a previously published method that uses a combination of Bloch and Landau-Zener evolution operators in Liouville space.[28,33,49,30] With this model, the computational time scales linearly with the number of spins. It has been improved to take into account large dipolar and exchange interactions[49] but also accurately describe the spin diffusion around the biradicals.[33]

The "multi-nuclei" model simulates an isolated biradical in interaction with many protons (from the radical and the solvent). This model uses as input MD simulations carried out in explicit TCE. It accounts for the presence of solvent protons but also biradical protons and their isotropic and anisotropic hyperfine couplings obtained by DFT. The simulations were carried out for both conformers and the polarization build-ups were weighted-averaged to mimic experimental results.

Nevertheless, it is important to note that the results obtained with the multi-nuclei model (build-up times and final polarization) do not consider the presence of intermolecular electron-electron couplings. Following our previous work,[33,49,30] we can use a second model, called the "box model" to correct the results obtained with the multi nuclei model. The "box" model uses *N* copies of a three-spin system (2 electrons, 1 proton) randomly distributed in a box to match a given biradical concentration. Assuming that "intermolecular" cross-effect is negligible, the effect of biradical concentration can be calculated by comparing the results of the box model with and without intermolecular electron-electron couplings. The simulated $\varepsilon_{\mathrm{on/off}}$, ε_{B} and $\varepsilon_{\mathrm{depo}}$ can be written as follows:

$$\varepsilon_X^{\mathrm{sim}} = \varepsilon_X^{\mathrm{multi-nuclei}} \times \frac{\varepsilon_X^{\mathrm{Box\ /\ Interacting}}}{\varepsilon_X^{\mathrm{Box\ /\ Isolated}}} = \varepsilon_X^{\mathrm{multi-nuclei}} \times R_X^{\mathrm{Box}}$$

Where R_X^{Box} corresponds to a correction factor accounting for the biradical concentration. This is justified for homogenously distributed biradicals in the tens of millimolar range as inter-molecular cross-effect rotor events are then particularly weak.[27,28,31] This approach has been shown to provide $\varepsilon_{\mathrm{on/off}}$, ε_{B} and $\varepsilon_{\mathrm{depo}}$ values that are relatively close to experimental ones for TEKPol, AMUPol and AsymPol-POK.[30,33] More details about the parameters used in the simulations can be found in the SI.

DFT simulations. Except otherwise specified, the DFT computation were carried out via Orca 5.0.[75] The preliminary structures were generated and optimized using Avogadro v1.2.[76] The structures were optimized using r2SCAN-3c.[77] A Polarizable Continuum Model Chloroform (PCM (Chloroform))[78] was used to mimic the dielectric properties of TCE. The *g*-tensors, dipolar interaction and hyperfine couplings were computed using PBE0,[79] def2-TZVP.[80] The hyperfine coupling to either electron *a* or *b* were computed, bearing in mind that accurate determination is beyond the scope of this article.[81] The Gauge origin problem was sorted out using the origin as the spin density. The exchange interaction was computed using the range-separated functional ωB97M-D4,[82,83] the def2-SVP basis, and a very tight and slow convergence (10^{-10} Hartree).[84]

EPR simulations. The EPR spectra were computed using Easyspin 5.2.20[85] via the Hamiltonian diagonalization method ("matrix"). The line broadening used, corresponding to a *g*-strain proportional to $[2(g_{xx}-2), g_{yy}-2, g_{zz}-2] \times 7\%$, and a mixture of Gaussian and Lorentzian lineshapes with linewidth of 0.4 and 0.4 mT respectively. The EPR spectra were fitted using the DFT-predicted parameters as starting points. The *g*-values

were first adjusted, and then the conformer ratio. Finally, *g*-tensors' Euler angles and the magnitude of the *J*-exchange interaction were refined together. The Euler angles of the dipolar interaction were fixed as they had very little impact on the fits. For the fitting procedure, a weighting factor of 1 for the 9.6 GHz (X-band) spectrum and of 2 for the 240 GHz spectrum was applied, giving thus a higher contribution of the high field EPR spectrum fit to the least-square sum and therefore forcing a better agreement with the high field spectrum with respect to the low field one for the extraction of the *g*-tensor relative orientation. Indeed, the low field EPR spectrum is dominated by the dipolar/exchange interaction and the ^{14}N hyperfine coupling while the high field spectrum is sensitive to the biradical geometry and *g*-tensor relative orientation. When multiple reasonable fits were obtained, the best one was chosen based on its match with the low field spectral features (resonant positions and relative intensities).

Molecular Dynamics (MD) simulations. MD simulations were carried out using OpenMM[86] and the AMBER[87] (GAFF2) force field. For the nitroxide, the force field derived by Barone's group[88] was adapted to match the GAFF2 atom type.[89] Lone pairs were added to NO in order to faithfully represent hydrogen bonding occurring in the solvent[88] and an additional dihedral angle was included in the force field as previously described.[90] The charges were obtained from the DFT structures, using the two-steps RESP fitting procedure with Multiwfn[91] to provide reliable MD structures. The MD simulations were carried out in explicit TCE (including bond rotation), whose charges were obtained on the same way. The MD simulations used as input for MAS-DNP simulations, consisted in first minimizing the energy of the molecular system, then equilibrating it for 20 ps, and finally propagating it for 100 ns in steps of 1 fs under an assumed pressure of 1 bar and a temperature of 298 K. The set temperature was then quickly decreased to 100 K over 400 ps to simulate freezing and glass formation.

Results and Discussion

The AsymPols are bisnitroxides made of a piperidine-based radical linked to a pyrrolinoxyl radical via an amide bridge.[45,49] AsymPol-TEK and cAsymPol-TEK (Figure 1) contain features that were previously introduced with bcTbK and TEKPol.[48] Specifically, spirocyclohexyl groups flank the nitroxide of the piperidine ring to slow the electron relaxation times, and phenyl groups contribute to higher solubility in organic solvents. The electron relaxation times of cAsymPol-TEK were further slowed down by introduction of spirocyclohexyl groups on the five-membered pyrroline ring, which also increase the molecular weight.[47,48,92,93]

Synthesis of AsymPol-TEK and cAsymPol-TEK

The synthesis of AsymPol-TEK and cAsymPol-TEK (Scheme 1) followed closely that of AsymPol.[45] Conjugation of nitroxide **1**[94] to 3-carboxy-pyrrolinoxyl **2**[95] provided AsymPol-TEK in good yields. HPLC analysis revealed the presence of two diastereomers. The origin of the stereoisomerism is the configuration of the two cyclohexane carbon atoms bearing the phenyl substituents. Relative to the cyclohexane rings, a phenyl group has either a cis- or trans-relationship to the nitrogen at the spirocycle junction. This can result in three diastereomers, namely the cis-cis, cis-trans and trans-trans. Only two diastereomers, named isomer A and isomer B, were observed and isolated by chromatography (Supporting Information). Isomer A (cis-cis) crystallized readily and the crystal structure showed that the two benzene rings were in equatorial position with respect to the cyclohexyl rings, with an "open-open" conformation relative to the N-O group (see SI).[96] In spite of several attempts, we were not able to crystallize isomer B. For AsymPol-TEK, except specified otherwise, all DNP experiments were conducted on isomer A. cAsymPol-TEK was synthesized in an analogous manner to AsymPol-TEK by condensation of **1** with spirocyclohexyl-3-carboxypyrrolinoxyl **3.**[95] In this case, only one peak was observed by HPLC analysis, indicating a single isomer. The crystal structure of cAsymPol-TEK revealed a cis-cis isomer in which the two benzene rings in are in equatorial positions with an "open-open" conformation relative to the N-O group (see SI).

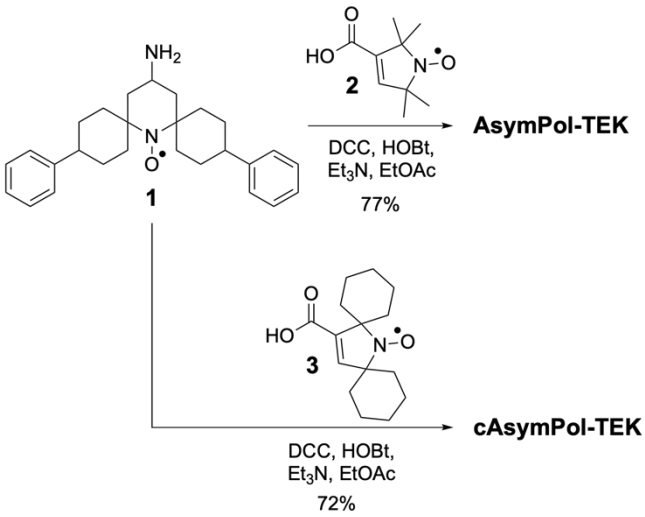

Scheme 1: Synthesis of AsymPol-TEK and cAsymPol-TEK.

Geometry of AsymPol-TEK and cAsymPol-TEK

The structures of the biradicals AsymPol-TEK and cAsymPol-TEK in frozen solution were determined using DFT calculations. After obtaining the idealized geometry of each biradical and the corresponding magnetic properties (*g*-tensors, exchange interaction and dipolar couplings), the latter were used as initial parameters to fit the EPR spectra.[49,30,33] While the planarity of the peptide bond (i.e. H-N-C=O) is maintained, the steric

hindrance between the N-H proton and the C=C-H proton of the five-membered ring prevents the carbonyl bond and the double bond (i.e. O=C-C=C) from being in the same plane. As a result, AsymPol-TEK and cAsymPol-TEK each contain two major conformers, dubbed **#1** and **#2**, that have a different relative orientation between the five and six membered rings, shown in Figure 2 for AsymPol-TEK.

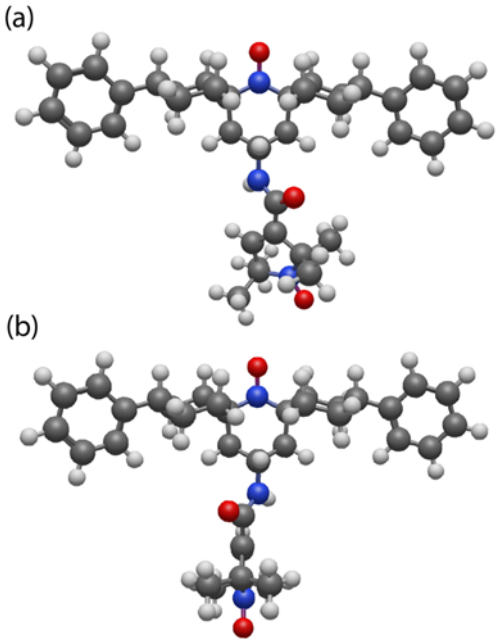

Figure 2 3D representation of the two open-open conformers of AsymPol-TEK (a) conformer #1, (b) conformer #2

The DFT simulations predict that conformer **#1** is slightly lower in energy than **#2**. The two conformers possess different magnetic properties: a larger *g*-tensors' distance, $L_{a,b}$, is predicted for **#2** vs **#1**, while the anti-ferromagnetic exchange interaction between the two unpaired electrons, $J_{a,b}$, is about +100 MHz for **#1** and +60 MHz for **#2**. Similar predictions were obtained for cAsymPol-TEK (Table 1).

To refine the predictions of the DFT calculations, the experimental EPR spectra, recorded at frequencies of 9.6 and 240 GHz, were fitted (see Figure 3a). At 9.6 GHz, the EPR spectra of AsymPol-TEK and cAsymPol-TEK are similar, but some minor differences are observed in the high-frequency EPR spectra. These differences are reproducible, despite variations in the glass quality. We note that the high-field EPR spectra differ significantly from those of the AsymPol-POKs in the g_{yy} region, revealing different properties between the POK and TEK versions.

The magnetic/geometric parameters predicted by DFT provided reasonable starting values for the fitting of the EPR spectra that yielded acceptable agreement with the experimental data (Table 1). Both biradicals present at least the two considered conformers (**#1** and **#2**) that have similar dipolar couplings (between 56 and 60 MHz), but different exchange interactions and different relative orientations. Conformers **#1** and **#2**, are present at a ratio of 60:40 for AsymPol-TEK and 65:35 for cAsymPol-TEK. For conformers **#1**, the exchange interactions were found to be 95 and 105 MHz for AsymPol-TEK and cAsymPol-TEK, respectively, and 65 and 60 MHz for conformers **#2** (see Table 1). These exchange couplings are slightly lower for AsymPol-TEK/cAsymPol-TEK compared to AsymPol-POK/cAsymPol-POK. This could already be inferred from the liquid-state EPR spectra, which presents a weaker exchange interaction of $|J_{a,b}|$ = 55 MHz (vs 78 MHz for AsymPol-POK) as shown in Figure S1. This is likely related to interaction with the different solvents, which impacts electron delocalization as revealed by the larger g_{xx} value that correlates with a shift of the unpaired spin-density towards the O (see **Table 1**). In addition, the relative orientation of the NO groups can affect the overlap between the orbitals of the unpaired electrons and thus the exchange interaction.

Table 1. List of the calculated (DFT) and fitted magnetic parameters for the AsymPol-TEK and cAsymPol-TEK biradicals.

Biradical	*g-tensors [g_{xx}, g_{yy}, g_{zz}]*	*g-tensors relative orientation [α, β, γ] [degrees]*	*Dipolar coupling, Exchange interaction [MHz]*	*Dipolar orientation [ϕ, θ] [degrees]*[a]	$L_{a,b}$ ($\times 10^3$)
*AsymPol-TEK #1 DFT/**Fit***	[2.0090, 2.0060, 2.0021; 2.0095, 2.0064, 2.0022] /	[98,148, 129]/**[115,150, 129]**	[58,96]/**[58,95]**	[-19,104]	4.2/**3.6**
*AsymPol-TEK #2 DFT/**Fit***	**[2.0086, 2.0062, 2.0023 ; 2.0095, 2.0062, 2.0024]**[b]	[75,85,89]/**[67,73,85]**	[56,61]/**[56,65]**	[-14, 94]	6.0/**5.8**
*cAsymPol-TEK #1 DFT/**Fit***	[2.0089, 2.0060, 2.0021; 2.0095, 2.0064, 2.0022] /	[116,149,152] /**[121,155, 150]**	[60,137]/**[60,105]**	[-20, 108]	4.8 / **4.1**
*cAsymPol-TEK #2 DFT/**Fit***	**[2.0089, 2.0060, 2.0022 ; 2.0098, 2.0061, 2.0024]** [b]	[76,86,93]/**[76,84,92]**	[56,67]/**[56,60]**	[-12.5, 96]	5.9 / **5.6**

a Euler angles are given with respect to the *g*-tensor of the five-membered ring, using Easyspin's v5 rotation convention (active rotation).
b We assumed identical *g*-tensors values for both conformers.

Journal Name

ARTICLE

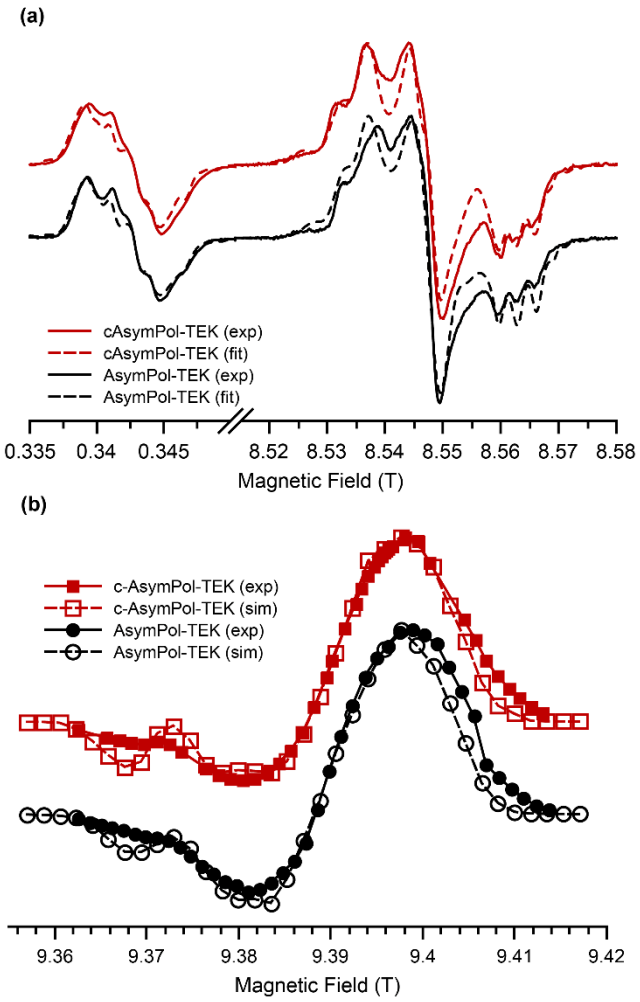

Figure 3 (a) Experimental (solid lines) and best fit (dashed lines) EPR spectra of AsymPol-TEK (black) and cAsymPol-TEK (red) in TCE with h-BN, measured at 100 K, 9.6 T and 240 GHz. Note that the experimental spectra are affected by the cooling process. This relates to the difficulty in obtaining a reproducible glassy state with TCE. For the fits, the ^{14}N hyperfine was set to [15,14,95] MHz for the five- and [18,17,98] MHz for the six-membered ring. (b) Experimental (full symbols) and simulated (open symbols) MAS-DNP field profiles of AsymPol-TEK (black circles) and cAsymPol-TEK (red squares) measured in TCE with h-BN at 100 K and 263 GHz.

The agreement between experiment and simulations was improved with the use of significant *g*-strain (larger than in previous studies),[49,97,30,33] but it remains imperfect. This is likely due both to the lack of precise control of the glass formation and to the fact that the AsymPol-TEK radicals possess a distribution of conformations, implying a distribution of exchange interactions.[84,98] The validity of the parameters extracted from the fits was confirmed by comparing experimental and simulated MAS-DNP field profiles (DNP enhancement versus magnetic field for a fixed μw frequency), which shows very good agreement (Figure 3b). The relative ratio between the positive and negative maxima of the DNP field profile is well reproduced, as well as the features at 9.37 T. The field-sweep profiles of AsymPol-TEK and cAsymPol-TEK are very similar to their POK counterparts. However, there are variations in the 9.36-9.39 T regions, confirming that the TEK versions have lower exchange interactions.[45]

MAS-DNP efficiency and reproducibility of measurements

The MAS-DNP efficiency of AsymPol-TEK and cAsymPol-TEK was investigated and compared to TEKPol. Hexagonal boron nitride (h-BN) was added to the solution to improve the microwave penetration and the DNP efficiency in TCE.[68]

To maximize the DNP enhancement, the nuclear spin-lattice relaxation should be slower than the rate at which the hyperpolarization is transferred throughout the system. This must be true for both the protons that are close to the radicals and also for the bulk ones.[21] In practice, it is possible to control to some extent the nuclear relaxation time for the bulk nuclei, $T_{1,n}^{Bulk}$. For example, it can be lengthened by sample degassing that removes paramagnetic O_2 from the solution.[68,99] *In situ* freeze-thaw cycles, via sample insert/eject at 100 K under N_2, has been shown to be an efficient way to remove dissolved O_2 in TCE.[21,60] Nevertheless, reproducibility is not always good when using TCE.[68] The main reason for this stems from the difficulty of forming a good glass in a reproducible manner, as indicated by the resulting ^{13}C NMR linewidth. [68] This prevents the sample formulation from being easily optimised and makes it more difficult to assess the comparative performance of polarizing agents.

TCE can form several phases upon cooling, an amorphous glass phase, and three crystalline phases (denoted α, β and γ) that can be obtained between 100 and 170 K.[100] The metastable crystalline γ-phase can be formed upon heating the glass phase to 140-150 K.[100] This is illustrated in Figure 4a and 4b, where the evolution of the ^{13}C CPMAS NMR spectrum as a function of the sample temperature is shown for both AsymPol-TEK and TEKPol. In these experiments, after a cold insertion, the temperature of the sample was gradually increased from 120 to 160 K. The TCE glass phase is preserved until 130 K, giving rise to a single broad resonance in the ^{13}C spectrum. The glass phase gradually converts into a crystalline phase in the 140-160 K range. This can be clearly seen with the appearance of resolved shoulders in the ^{13}C TCE spectrum, corresponding to the dipolar coupling between the ^{13}C and the ^{35}Cl/^{37}Cl nuclei. We believe that we might be forming the metastable γ-phase, recently reported in the literature.[100] Upon cooling the sample back from

160 to 110 K, it results in the formation of the thermodynamically stable crystalline β-phase,[99] and inevitably gives rise to a reduction in DNP performance (as compared to the glass phase at the same temperature).[68]

To reproducibly obtain amorphous glass for TCE, we modified our experimental protocol (see material and methods) to minimize the stator temperature at sample insertion. This implies flushing cold nitrogen gas inside the empty stator and turning off the μw irradiation before insertion. This protocol ensures a consistent glass formation, as shown for the ^{13}C CPMAS TCE spectra at 9.4 T (for 16 mM TEKPol, AsymPol-TEK and cAsymPol-TEK) during the freeze-thaw cycles procedure (Figure 5). All spectra correspond to the formation of a glass (no crystalline phase observed at any point in the cycle). This modified protocol significantly improves the reproducibility of the DNP measurement with TCE.

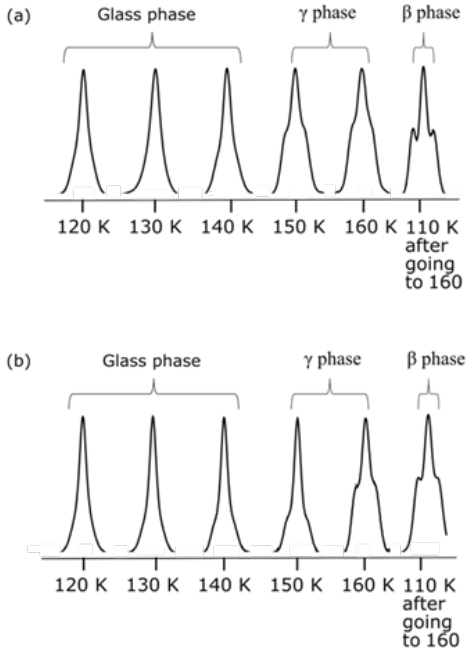

Figure 4. ^{13}C CP-MAS spectra (9.4 T) of 16 mM radical solutions of (a) AsymPol-TEK and (b) TEKPol in TCE in the presence of h-BN, as a function of the temperature. For better comparison of the lineshapes, all spectra are scaled to the same intensity. The last spectrum was obtained after slowly cooling back the sample from 160 K to 110 K.

The effect of the oxygen removal on the ^1H TCE $T_{1,n}^{Bulk}$ can be seen in Figure 6d. For this undoped TCE sample, ^1H $T_{1,n}^{Bulk}$ increases from ~2.5 s, measured after the first freezing of the solution, to ~ 70 s after 7 freeze-thaw cycles. The sensitivity at 9.4 T for each biradical as a function of the number of freeze-thaw cycles is given Figure 6a. Over the course of 6 insert-ejects, the sensitivity increases moderately for all biradicals. cAsymPol-TEK provides a higher sensitivity (normalized to one) than AsymPol-TEK (0.8), while TEKPol is less sensitive (0.6-0.7). This behaviour is in sharp contrast with the corresponding DNP enhancement, $\epsilon_{on/off}$ (Figure 6c), which for TEKPol, increases from 140 to 307 between the first and the sixth freeze-thaw cycle. In contrast, $\epsilon_{on/off}$ of AsymPol-TEK and cAsymPol-TEK varies much less, starting at ~60 to end at 75 and 87, respectively, after 6 cycles. The stronger change in $\epsilon_{on/off}$ for TEKPol is in part due to increased depolarization due to the lengthening of ^1H bulk T_1, as seen through the decrease in signal intensity in the absence of microwave irradiation (Figure 6). This effect is not present for the AsymPol-TEK PAs.

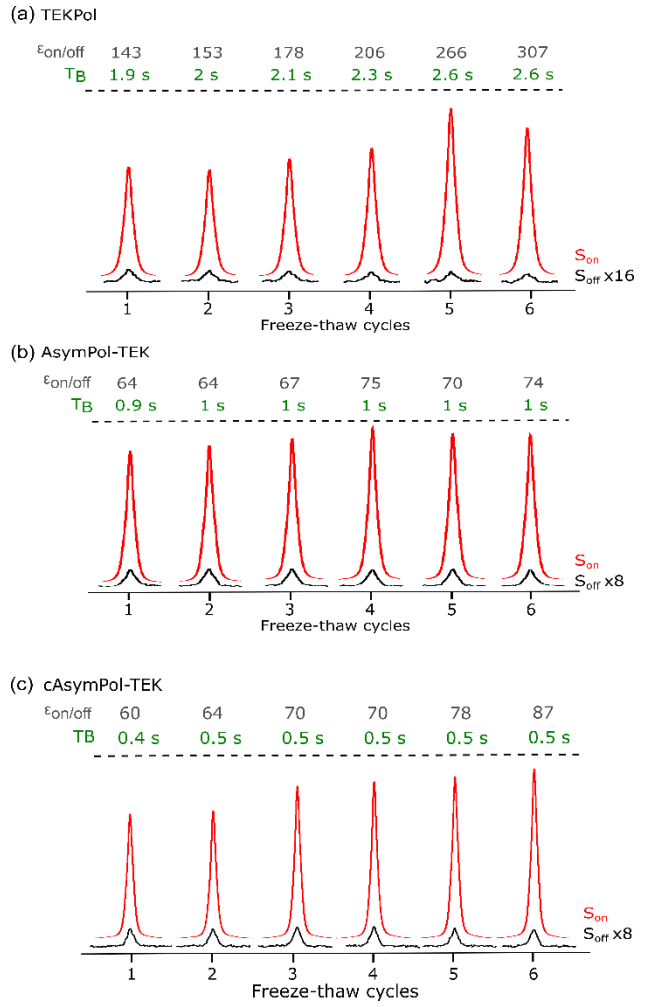

Figure 5. ^{13}C CP-MAS spectra of 16 mM radical solution of (a) TEKPol, (b) AsymPol-TEK, and (c) cAsymPol-TEK in TCE mixed with h-BN, as a function of the number of freeze-thaw cycles with (red) and without (black) μw irradiation, using a 3.2 mm rotor at 9.4 T, 8 kHz MAS frequency and 105 K. The ^{13}C CP-MAS spectra were acquired with a recycle delay of $1.3 \cdot T_B$. The evolution of the normalized sensitivity, the build-up time T_B , and $\epsilon_{on/off}$ as a function of the number of freeze-thaw cycles can be compared for the 3 radicals in Figure 6.

The stronger dependence of $\epsilon_{on/off}$ on the number of freeze-thaw cycles for TEKPol may also come from its longer DNP build-up time, T_B, compared to the AsymPol-TEKs. Interestingly, as seen in Figure 6b, values of T_B are quite stable for the AsymPol-TEK radicals, with $T_B \approx 1$ s for AsymPol-TEK and 0.5 s for

cAsymPol-TEK at 9.4 T, while they are clearly increasing for TEKPol from 1.9 to 2.6 s over 6 freeze-thaw cycles. This suggests that the polarization build-up of the AsymPol-TEK PAs is less sensitive to the lengthening of $T_{1,n}^{\mathrm{Bulk}}$ than that of TEKPol.

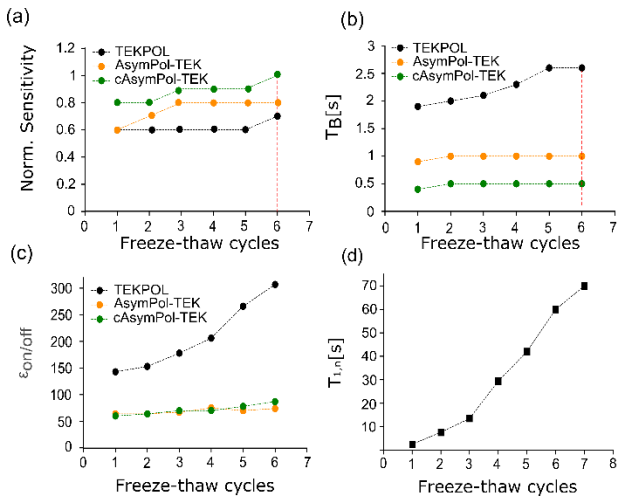

Figure 6. (a) Normalized sensitivity ($S_{on}/\sqrt{T_B}$), (b) build-up time T_B and (c) $\epsilon_{on/off}$ values for 16 mM TEKPol (black), AsymPol-TEK (orange), and cAsymPol-TEK (green) in TCE mixed with h-BN, as a function of the number of freeze-thaw cycles. (d) Evolution of the proton longitudinal relaxation time $T_{1,n}$ for pure TCE (no radicals) as a function of the number of freeze-thaw cycles. All experiments were performed using a 3.2 mm rotor at 9.4 T, 8 kHz MAS frequency and 105 K.

Overall, the results reported here for TEKPol are consistent with previous reports,[60,66,72] keeping in mind that $\epsilon_{\mathrm{on/off}}$ factors do not correlate directly with NMR sensitivity. Similar experiments were also conducted at 14.1 T. The DNP performance of the three PAs is summarized in Table 2, at both 9.4 and 14.1 T. For this comparison, the reported values of $\varepsilon_{\mathrm{on/off}}$ and T_B correspond to the best sensitivity among each freeze-thaw series. At 14.1 T, TEKPol at 10 mM leads to $\epsilon_{\mathrm{on/off}}$ = 122 and $T_B = 9.1$ s, and at 16 mM $\epsilon_{\mathrm{on/off}}$ = 128 and $T_B = 6.3$ s after 6 freeze thaw cycles but also leads to significant depolarization with ϵ_{depo}~0.6 (at 10 mM). AsymPol-TEK and cAsymPol-TEK at 10 mM led to lower $\epsilon_{\mathrm{on/off}}$, 74 and 80 respectively but with a much shorter $T_B \approx 2$ s. Once the depolarization has been accounted for (ϵ_{depo}~0.75 for both AsymPol-TEKs), AsymPol-TEK and cAsymPol-TEK yield 1.75- and 2.5-times higher sensitivity than TEKPol, respectively. All in all, the AsymPol-TEK PAs clearly yield higher sensitivity than TEKPol at both fields, with a more pronounced improvement for the methyl-free cAsymPol-TEK and at the higher magnetic field. We note here that the polarization build-up curve of AsymPol-TEK in presence of μw is not purely mono-exponential, but slightly bi- or stretched exponential.

Table 2. Experimental and simulated DNP performance of TEKPol, AsymPol-TEK and cAsymPol-TEK in TCE mixed with h-BN, at 9.4 T (16 mM) and 14.1 T (10 and 16 mM), and 8 kHz MAS.

9.4 T	$T_B[s]$[b]	$\mathcal{E}_{\mathrm{on/off}}$[b]	Sensitivity[a]
TEKPol (16 mM) (exp/**sim**)	2.6/**3.2**	307/**300**	0.7
AsymPol-TEK (16 mM) (exp/**sim**)	1 / **0.7**	75/**115**	0.8
cAsymPol-TEK (16 mM) (exp/**sim**)	0.5 / **0.7**	87/**136**	1
14.1 T			
TEKPol (10 mM) (exp/**sim**)	9.1/**7.6**	122/**128**	0.4
TEKPol (16 mM) (exp/**sim**)	6.3/**4.8**	128/**165**	0.45
AsymPol-TEK (10 mM) (exp/**sim**)	2.3/**1.8**	74/**73**	0.7
cAsymPol-TEK (10 mM) (exp/**sim**)	1.8/**2**	80/**89**	1

[a] The sensitivity is normalized to the highest value.

[b] Light numbers are experimental values. Outcome of MAS-DNP simulations are in bold.

The experimental performance of the different radicals was compared to MAS-DNP simulations (Table 2). For all PAs, the build-up times are relatively well reproduced by simulations at both magnetic fields. The DNP enhancement for TEKPol is also well reproduced for 16 mM concentration at 9.4 T and 10 mM at 14.1 T but it is overestimated for 16 mM at 14.1 T. The concentration trend at 14.1 T is consistent, with the simulations predicting that 10 mM TEKPol yields a slower build-up time than 16 mM. This confirms the robustness of the model used for the simulations. For AsymPol-TEK and cAsymPol-TEK, the predicted values of T_B are very close to the experimental data at both fields, whereas the DNP enhancements are slightly overestimated at 9.4 T but well reproduced at 14.1 T. A better agreement between simulations and experiment could be obtained by adjusting the electron and nuclear relaxation times. However, we preferred to keep the same nuclear relaxation times for all PAs (both for the protons close to the biradicals and for the bulk ones). This highlights the origin of the fast build-up times of the AsymPol-TEK radicals, namely the stronger e-e couplings (dipolar and *J*-exchange interaction) compared to TEKPol, in line with the results reported for the water-soluble members the AsymPol family.[45,49]

The improved DNP sensitivity yielded by both AsymPol-TEK and cAsymPol-TEK is directly related to the shorter build-up time T_B, as compared to TEKPol. The higher values of $\varepsilon_{\mathrm{on/off}}$ obtained with TEKPol (Figure 6c) are related to its stronger depolarization, with $\varepsilon_{\mathrm{depo}}$ around 0.5 both at 9.4 and 14.1 T at 16 mM concentration (see Table S2), which led to a significant overestimation of the hyperpolarization gain. The situation is very different for the AsymPol-TEKs, that exhibit a smaller depolarization effect ($\varepsilon_{\mathrm{depo}}$ = 0.9-0.8 at 16 mM and 9.4 T; 0.75 at 10 mM and 14.1 T), which is another important characteristic of the AsymPol PAs.[45,49]

Open and close biradicals

So far, all the experiments reported for AsymPol-TEK were performed with isomer A, where phenyl groups are in an equatorial position with an "open-open" conformation.

Please do not adjust margins

However, changing the configuration at the carbons connected to the phenyl groups can give two other stereoisomers, shown in Figure 7. A ring flip of the cyclohexyl ring will place the phenyl group in the more accommodating equatorial group and move the cyclohexyl closer to the nitroxide, giving a "closed" conformation. Thus, the two isomers, other than isomer A, that are possible will adopt either an “open-close” or a “close-close” structure. Although we were not able to crystallise isomer B, we assume that it corresponds to the “open-closed” isomer as it is lower in energy than the "closed-closed" structure.

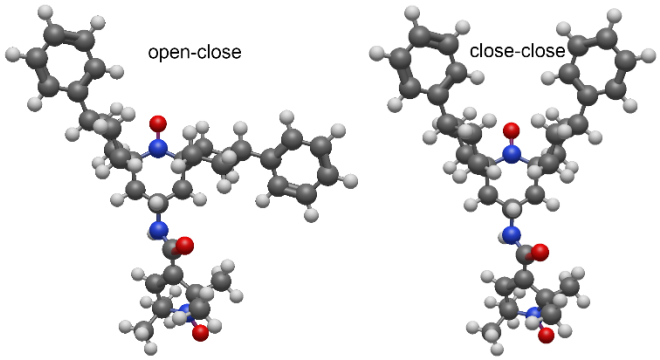

Figure 7. 3D structures of the open-closed (left) and closed-closed (right) isomers of AsymPol-TEK.

The MAS-DNP performance of the AsymPol-TEK “open-close” isomer B (Figure 7) was found to be far inferior to the “open-open” isomer A, with $\epsilon_{\mathrm{on/off}} \approx 33$ and $T_B = 0.4$ s at 9.4 T and $\epsilon_{\mathrm{on/off}} \approx 32$ and $T_B = 1.9$ s at 14.1 T. DFT simulations of isomer B yielded two conformers with unfavourable relative orientation of the *g*-tensors ($L_{a,b} = 4.7 \times 10^{-3}$). Moreover, the predicted exchange interaction is larger ($J_{a,b} \approx 140$ MHz). Both characteristics, unfavourable *g*-tensor relative orientation and too strong exchange interaction, explain the poor DNP performance of isomer B.

The “closed-closed” conformation, even though not obtained in the synthesis, can also be explored in-silico. The relative “distance” of the *g*-tensors is higher ($L_{a,b} = 5.8 \times 10^{-3}$), equivalent to the (better) conformer #2 of isomer A. However, the predicted exchange interaction is significantly higher with $J_{a,b} \approx 250$ MHz. This would make MAS-DNP very inefficient at lower fields, as $|2J_{a,b}| > \nu_n$, but could potentially be of interest at higher fields.

Applications

The efficiency of the AsymPol-TEKs was tested by hyperpolarizing proton-dense microcrystals of adenosine and caffeine at 9.4 T and 105 K (see Table S3). Overall, cAsymPol-TEK yields a higher sensitivity (signal-to-noise ratio per square root of time) compared to AsymPol-TEK and TEKPol, both for adenosine and caffeine microcrystals (Figure 8a-b). As expected, the sensitivity under microwave irradiation is higher for adenosine than caffeine microcrystals owing to the shorter ^{1}H bulk $T_{1,n}$ of the latter. Note that we did not optimize the radical or solvent proton concentration here.[49] Using a biradical concentration of 10 mM, cAsymPol-TEK provides about x2.5 to x4 improvement in time-savings for adenosine and caffeine microcrystals respectively. This allows recording DQ/SQ ^{13}C-^{13}C correlation experiments at natural isotopic abundance in a few hours using cAsymPol-TEK. Figure 8c shows a 2D experiment with high S/N recorded in 10 h on adenosine microcrystals. Thanks to the mixing time chosen, one can clearly detect polarization transfer corresponding to carbon spins distant by one, two and three-bond. Figure S2 shows that in the more challenging case of caffeine, it is possible to get clear cross-peaks in about one hour of experimental time. A third example of DQ/SQ ^{13}C-^{13}C correlation experiments at the higher magnetic field of 14.1 T on histidine at natural isotopic abundance using AsymPol-TEK can be found in Figure S3.

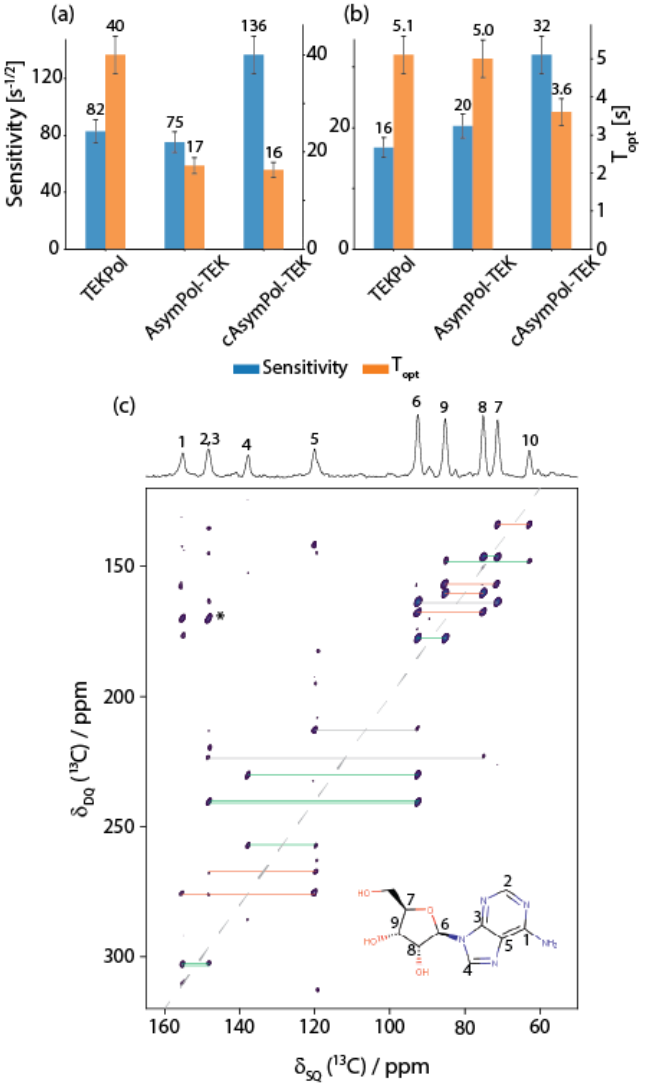

Please do not adjust margins

Figure 8. (a)-(b) Signal-to-noise ratio per square root of the experimental time (in blue) and optimal recycle delay T_{opt} (in orange) of (a) adenosine and (b) caffeine powders impregnated with 10 mM TEKPol, AsymPol-TEK and cAsymPol-TEK in TCE. (c) DNP-enhanced 2D ^{13}C-^{13}C DQ-SQ correlation spectra of adenosine microcrystals at NA using cAsymPol-TEK. The experiment was acquired using SR26 as dipolar recoupling sequence, at 6.6 kHz MAS, 105 K and 9.4 T. Experimental time was 10 h and the total mixing time for SR26 was 4.8 ms. ^{13}C-^{13}C correlations are mapped out on the 2D spectra, in orange for one-bond correlations, green for two-bonds, and grey for ≥ three-bonds. Spinning side bands are indicated with asterisks. The chemical structure of adenosine with numbering of the carbon atoms is given as inset.

Finally, we also used TEKPol, AsymPol-TEK and cAsymPol-TEK to polarize the surface of semiconducting nanocrystals. More specifically, we chose ZnO nanocrystals coated by mono-anionic diphenyl phosphate (DPP) ligands, that were synthetized using an one-pot self-supporting organometallic (OSSOM) approach.[101,102] Details of the synthesis can be found in the SI. Figure 9 shows the NMR sensitivity and the proton build-up time T_B for the ZnO NCs impregnated with TCE. The AsymPol-TEKs yield an improvement in sensitivity over TEKPol, which translates into a x9 in time-saving for cAsymPol-TEK. These results open interesting prospects for the study of challenging materials (bulk and surface) by MAS-DNP.

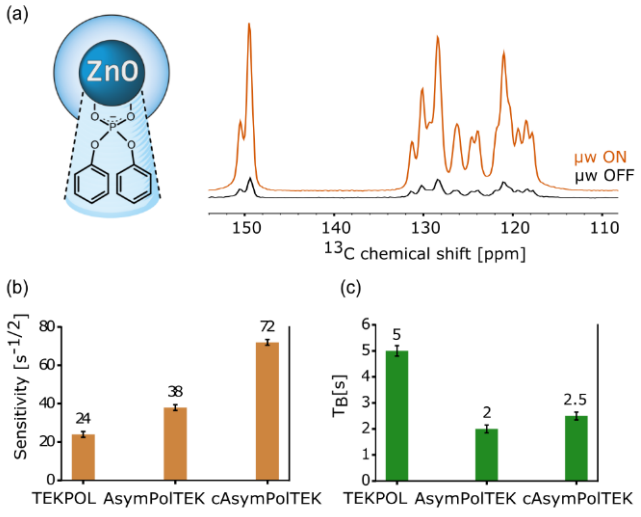

Figure 9. (a) {^{1}H-}^{13}C CPMAS spectra of ZnO-DPP NCs impregnated with 10 mM cAsymPol-TEK in TCE with (orange) and without (black) μw irradiation. (b) Sensitivity and (c) proton T_B of ZnO-DPP NCs impregnated with 10 mM TEKPol, AsymPol-TEK and cAsymPol-TEK in TCE. $\varepsilon_{on/off}$ values were 9 for TEKPol, 6 for AsymPol-TEK, and 10 for cAsymPol-TEK. All data were recorded at 9.4 T, 8 kHz MAS frequency and 105 K.

Conclusions

In summary, we have introduced two new members of the AsymPol family for non-aqueous applications, named AsymPol-TEK and cAsymPol-TEK. Both PAs provide improved sensitivity compared to TEKPol at both 9.4 and 14.1 T. By ensuring that the TCE-based DNP sample is always introduced into a probe head with a temperature around 100 K or below, the reproducibility of the DNP measurements with TCE can be significantly improved. The efficiency of these PAs can be rationalized using a combination of DFT, MD, EPR and MAS-DNP simulations that reveal the presence of two major conformers. In addition, these results show that the introduction of the spirocyclohexyl groups does not significantly change the linker geometry, nor the e-e spin couplings involved. Thus, the improved performance of cAsymPol-TEK relative to AsymPol-TEK is attributed to the replacement of methyl groups with cyclohexyl groups, which tends to lengthen both the electron and the core protons relaxation times, leading to better CE-DNP efficiency.

The key advantage of the AsymPol-TEK PAs lies not only in their high polarization gain but also in their fast hyperpolarization build-up times. This makes them ideal to polarize proton-dense systems, and/or systems with short intrinsic ^{1}H nuclear relaxation times. This is illustrated with the acquisition of ^{13}C-^{13}C correlation experiments at natural isotopic abundance of organic microcrystals, and to polarize ligands at the surface of ZnO nanocrystals.

Conflicts of interest

There are no conflicts to declare.

Acknowledgements

This work was supported by the French National Research Agency (CBH-EUR-GS and Labex ARCANE ANR-17-EURE-0003, Glyco@Alps ANR-15-IDEX-02) and the European Research Council Grant ERC-CoG-2015 No. 682895 to G. D. P. Part of this work, carried out on the Platform for Nanocharacterisation (PFNC), was supported by the "Recherches Technologiques de Base" program of the French National Research Agency (ANR). This work was supported by the Icelandic Research Fund, grant No. 239662, the University of Iceland Research Fund (S.Th.S) and a doctoral fellowship from the University of Iceland Research Fund (SC). T.H. thanks the Deutsche Forschungsgemeinschaft (DFG) for a postdoctoral fellowship (414196920). F.M.V. thanks Carl Fleischer for the histidine sample. The National High Magnetic Field Laboratory is supported by the NSF (DMR-1644779 and DMR-2128556) and by the State of Florida. The 14.1 T MAS-DNP system at NHMFL is funded in part by NIH S10 OD018519 (magnet and console), and NIH P41 GM122698 and RM1-GM148766.

References

1 Q. Z. Ni, E. Daviso, T. V. Can, E. Markhasin, S. K. Jawla, T. M. Swager, R. J. Temkin, J. Herzfeld and R. G. Griffin, High

Please do not adjust margins

Frequency Dynamic Nuclear Polarization, *Accounts of Chemical Research*, 2013, **46**, 1933–1941.
2 A. S. Lilly Thankamony, J. J. Wittmann, M. Kaushik and B. Corzilius, Dynamic nuclear polarization for sensitivity enhancement in modern solid-state NMR, *Progress in Nuclear Magnetic Resonance Spectroscopy*, 2017, **102–103**, 120–195.
3 S. Hediger, D. Lee, F. Mentink-Vigier and G. De Paëpe, in *eMagRes*, John Wiley & Sons, Ltd, 2018, pp. 105–116.
4 A. B. Barnes, G. De Paëpe, P. C. A. van der Wel, K.-N. Hu, C.-G. Joo, V. S. Bajaj, M. L. Mak-Jurkauskas, J. R. Sirigiri, J. Herzfeld, R. J. Temkin and R. G. Griffin, High-Field Dynamic Nuclear Polarization for Solid and Solution Biological NMR, *Applied Magnetic Resonance*, 2008, **34**, 237–263.
5 K. Kundu, F. Mentink-Vigier, A. Feintuch and S. Vega, in *eMagRes*, John Wiley & Sons, Ltd, 2019, pp. 295–338.
6 T. V. Can, Q. Z. Ni and R. G. Griffin, Mechanisms of dynamic nuclear polarization in insulating solids, *Journal of Magnetic Resonance*, 2015, **253**, 23–35.
7 K.-N. Hu, H. Yu, T. M. Swager and R. G. Griffin, Dynamic Nuclear Polarization with Biradicals, *Journal of the American Chemical Society*, 2004, **126**, 10844–10845.
8 C. Song, K. N. Hu, C. G. Joo, T. M. Swager and R. G. Griffin, TOTAPOL: A biradical polarizing agent for dynamic nuclear polarization experiments in aqueous media, *Journal of the American Chemical Society*, 2006, **128**, 11385–11390.
9 K. Jaudzems, T. Polenova, G. Pintacuda, H. Oschkinat and A. Lesage, DNP NMR of biomolecular assemblies, *Journal of Structural Biology*, 2019, **206**, 90–98.
10 A. J. Rossini, C. M. Widdifield, A. Zagdoun, M. Lelli, M. Schwarzwälder, C. Copéret, A. Lesage and L. Emsley, Dynamic nuclear polarization enhanced NMR spectroscopy for pharmaceutical formulations, *Journal of the American Chemical Society*, 2014, **136**, 2324–2334.
11 Diego Gauto, Ons Dakhlaoui, Ildefonso Marin-Montesinos, Sabine Hediger and G. D. Paëpe, Targeted DNP for biomolecular solid-state NMR, *Chemical Science*, 2021, **12**, 6223–6237.
12 B. Plainchont, P. Berruyer, J.-N. Dumez, S. Jannin and P. Giraudeau, Dynamic Nuclear Polarization Opens New Perspectives for NMR Spectroscopy in Analytical Chemistry, *Analytical Chemistry*, 2018, **90**, 3639–3650.
13 W. Y. Chow, G. De Paëpe and S. Hediger, Biomolecular and Biological Applications of Solid-State NMR with Dynamic Nuclear Polarization Enhancement, *Chem. Rev.*, 2022, **122**, 9795–9847.
14 N. Ghassemi, A. Poulhazan, F. Deligey, F. Mentink-Vigier, I. Marcotte and T. Wang, Solid-State NMR Investigations of Extracellular Matrixes and Cell Walls of Algae, Bacteria, Fungi, and Plants, *Chem. Rev.*, 2022, **122**, 10036–10086.
15 T. Biedenbänder, V. Aladin, S. Saeidpour and B. Corzilius, Dynamic Nuclear Polarization for Sensitivity Enhancement in Biomolecular Solid-State NMR, *Chem. Rev.*, 2022, **122**, 9738–9794.
16 A. J. Rossini, A. Zagdoun, M. Lelli, A. Lesage, C. Cop, L. Emsley, C. Copéret and L. Emsley, Dynamic Nuclear Polarization Surface Enhanced NMR Spectroscopy, *Accounts of Chemical Research*, 2013, **46**, 1942–1951.
17 D. Lee, S. Hediger and G. De Paepe, Is solid-state NMR enhanced by dynamic nuclear polarization?, *Solid State Nucl. Magn. Reson.*, 2015, **66–67**, 6–20.
18 F. A. Perras, T. Kobayashi and M. Pruski, Growing signals from the noise: Challenging nuclei in materials DNP, *eMagRes*, 2018, **7**, 35–50.
19 A. G. M. Rankin, J. Trébosc, F. Pourpoint, J. P. Amoureux and O. Lafon, Recent developments in MAS DNP-NMR of materials, *Solid State Nucl. Magn. Reson.*, 2019, **101**, 116–143.
20 Ü. Akbey, W. T. Franks, A. Linden, M. Orwick-Rydmark, S. Lange and H. Oschkinat, in *Hyperpolarization Methods in NMR Spectroscopy*, ed. L. T. Kuhn, Springer Berlin Heidelberg, Berlin, Heidelberg, 2013, vol. 338, pp. 181–228.
21 B. Corzilius, L. B. Andreas, A. A. Smith, Q. Z. Ni and R. G. Griffin, Paramagnet induced signal quenching in MAS–DNP experiments in frozen homogeneous solutions, *Journal of Magnetic Resonance*, 2014, **240**, 113–123.
22 H. Takahashi, C. Fernández-de-Alba, D. Lee, V. Maurel, S. Gambarelli, M. Bardet, S. Hediger, A.-L. Barra and G. De Paëpe, Optimization of an absolute sensitivity in a glassy matrix during DNP-enhanced multidimensional solid-state NMR experiments, *Journal of Magnetic Resonance*, 2014, **239**, 91–99.
23 T. Kobayashi, O. Lafon, A. S. Lilly Thankamony, I. I. Slowing, K. Kandel, D. Carnevale, V. Vitzthum, H. Vezin, J.-P. Amoureux, G. Bodenhausen and M. Pruski, Analysis of sensitivity enhancement by dynamic nuclear polarization in solid-state NMR: a case study of functionalized mesoporous materials, *Phys. Chem. Chem. Phys.*, 2013, **15**, 5553.
24 A. J. Rossini, A. Zagdoun, M. Lelli, D. Gajan, F. Rascón, M. Rosay, W. E. Maas, C. Copéret, A. Lesage and L. Emsley, One hundred fold overall sensitivity enhancements for Silicon-29 NMR spectroscopy of surfaces by dynamic nuclear polarization with CPMG acquisition, *Chem. Sci.*, 2012, **3**, 108–115.
25 K. R. Thurber and R. Tycko, Theory for cross effect dynamic nuclear polarization under magic-angle spinning in solid state nuclear magnetic resonance: The importance of level crossings, *The Journal of Chemical Physics*, 2012, **137**, 084508.
26 F. Mentink-Vigier, U. Akbey, Y. Hovav, S. Vega, H. Oschkinat and A. Feintuch, Fast passage dynamic nuclear polarization on rotating solids, *J. Magn. Reson.*, 2012, **224**, 13–21.
27 F. Mentink-Vigier, Ü. Akbey, H. Oschkinat, S. Vega and A. Feintuch, Theoretical aspects of Magic Angle Spinning - Dynamic Nuclear Polarization, *Journal of Magnetic Resonance*, 2015, **258**, 102–120.
28 F. Mentink-Vigier, S. Vega and G. De Paëpe, Fast and accurate MAS–DNP simulations of large spin ensembles, *Physical Chemistry Chemical Physics*, 2017, **19**, 3506–3522.
29 F. Mentink-Vigier, Optimizing nitroxide biradicals for cross-effect MAS-DNP: The role of: G -tensors' distance, *Physical Chemistry Chemical Physics*, 2020, **22**, 3643–3652.
30 F. Mentink-Vigier, A.-L. Barra, J. van Tol, S. Hediger, D. Lee and G. De Paëpe, *De novo* prediction of cross-effect efficiency for magic angle spinning dynamic nuclear polarization, *Phys. Chem. Chem. Phys.*, 2019, **21**, 2166–2176.
31 K. R. Thurber and R. Tycko, Perturbation of nuclear spin polarizations in solid state NMR of nitroxide-doped samples by magic-angle spinning without microwaves, *The Journal of Chemical Physics*, 2014, **140**, 184201.
32 A. Equbal, A. Leavesley, S. K. Jain and S. Han, Cross-Effect Dynamic Nuclear Polarization Explained: Polarization,

Please do not adjust margins

Please do not adjust margins

Depolarization, and Oversaturation, *J. Phys. Chem. Lett.*, 2019, **10**, 548–558.
33 F. Mentink-Vigier, T. Dubroca, J. Van Tol and S. Th. Sigurdsson, The distance between g-tensors of nitroxide biradicals governs MAS-DNP performance: The case of the bTurea family, *Journal of Magnetic Resonance*, 2021, **329**, 107026.
34 F. Mentink-Vigier, S. Paul, D. Lee, A. Feintuch, S. Hediger, S. Vega and G. De Paëpe, Nuclear depolarization and absolute sensitivity in magic-angle spinning cross effect dynamic nuclear polarization, *Phys. Chem. Chem. Phys.*, 2015, **17**, 21824–21836.
35 M. Rosay, L. Tometich, S. Pawsey, R. Bader, R. Schauwecker, M. Blank, P. M. Borchard, S. R. Cauffman, K. L. Felch, R. T. Weber, R. J. Temkin, R. G. Griffin and W. E. Maas, Solid-state dynamic nuclear polarization at 263 GHz: spectrometer design and experimental results, *Phys. Chem. Chem. Phys.*, 2010, **12**, 5850.
36 M. Rosay, M. Blank and F. Engelke, Instrumentation for solid-state dynamic nuclear polarization with magic angle spinning NMR, *Journal of Magnetic Resonance*, 2016, **264**, 88–98.
37 E. Bouleau, P. Saint-Bonnet, F. Mentink-Vigier, H. Takahashi, J.-F. Jacquot, M. Bardet, F. Aussenac, A. Purea, F. Engelke, S. Hediger, D. Lee and G. De Paëpe, Pushing NMR sensitivity limits using dynamic nuclear polarization with closed-loop cryogenic helium sample spinning, *Chem. Sci.*, 2015, **6**, 6806–6812.
38 Y. Matsuki, K. Ueda, T. Idehara, R. Ikeda, I. Ogawa, S. Nakamura, M. Toda, T. Anai and T. Fujiwara, Helium-cooling and -spinning dynamic nuclear polarization for sensitivity-enhanced solid-state NMR at 14T and 30K, *Journal of Magnetic Resonance*, 2012, **225**, 1–9.
39 D. Lee, E. Bouleau, P. Saint-Bonnet, S. Hediger and G. De Paëpe, Ultra-low temperature MAS-DNP, *Journal of Magnetic Resonance*, 2016, **264**, 116–124.
40 Y. Matsuki, S. Nakamura, S. Fukui, H. Suematsu and T. Fujiwara, Closed-cycle cold helium magic-angle spinning for sensitivity-enhanced multi-dimensional solid-state NMR, *Journal of Magnetic Resonance*, 2015, **259**, 76–81.
41 K. R. Thurber, A. Potapov, W.-M. Yau and R. Tycko, Solid state nuclear magnetic resonance with magic-angle spinning and dynamic nuclear polarization below 25 K, *J. Magn. Reson.*, 2012, **226**, 100–106.
42 K. Thurber and R. Tycko, Low-temperature dynamic nuclear polarization with helium-cooled samples and nitrogen-driven magic-angle spinning, *Journal of Magnetic Resonance*, 2016, **264**, 99–106.
43 D. A. Hall, D. C. Maus, G. J. Gerfen, S. J. Inati, L. R. Becerra, F. W. Dahlquist and R. G. Griffin, Polarization-Enhanced NMR Spectroscopy of Biomolecules in Frozen Solution, *Science*, 1997, **276**, 930–932.
44 Y. Matsuki, S. Nakamura, F. Hobo, Y. Endo, H. Takahashi, H. Suematsu and T. Fujiwara, Cryogenic signal amplification combined with helium-temperature MAS DNP toward ultimate NMR sensitivity at high field conditions, *Journal of Magnetic Resonance*, 2022, **335**, 107139.
45 F. Mentink-Vigier, I. Marin-Montesinos, A. P. Jagtap, T. Halbritter, J. van Tol, S. Hediger, D. Lee, S. Th. Sigurdsson and G. De Paëpe, Computationally Assisted Design of Polarizing Agents for Dynamic Nuclear Polarization Enhanced NMR: The AsymPol Family, *Journal of the American Chemical Society*, 2018, **140**, 11013–11019.
46 A. Lund, G. Casano, G. Menzildjian, M. Kaushik, G. Stevanato, M. Yulikov, R. Jabbour, D. Wisser, M. Renom-Carrasco, C. Thieuleux, F. Bernada, H. Karoui, D. Siri, M. Rosay, I. V. Sergeyev, D. Gajan, M. Lelli, L. Emsley, O. Ouari and A. Lesage, TinyPols: A family of water-soluble binitroxides tailored for dynamic nuclear polarization enhanced NMR spectroscopy at 18.8 and 21.1 T, *Chemical Science*, 2020, **11**, 2810–2818.
47 C. Sauvée, M. Rosay, G. Casano, F. Aussenac, R. T. Weber, O. Ouari and P. Tordo, Highly efficient, water-soluble polarizing agents for dynamic nuclear polarization at high frequency, *Angewandte Chemie - International Edition*, 2013, **52**, 10858–10861.
48 A. Zagdoun, G. Casano, O. Ouari, M. Schwarzwälder, A. J. Rossini, F. Aussenac, M. Yulikov, G. Jeschke, C. Copéret, A. Lesage, P. Tordo and L. Emsley, Large Molecular Weight Nitroxide Biradicals Providing Efficient Dynamic Nuclear Polarization at Temperatures up to 200 K, *Journal of the American Chemical Society*, 2013, **135**, 12790–12797.
49 R. Harrabi, T. Halbritter, F. Aussenac, O. Dakhlaoui, J. van Tol, K. K. Damodaran, D. Lee, S. Paul, S. Hediger, F. Mentink-Vigier, S. Th. Sigurdsson and G. De Paëpe, Highly Efficient Polarizing Agents for MAS-DNP of Proton-Dense Molecular Solids, *Angewandte Chemie International Edition*, 2022, **61**, e202114103.
50 G. Mathies, M. A. Caporini, V. K. Michaelis, Y. Liu, K.-N. Hu, D. Mance, J. L. Zweier, M. Rosay, M. Baldus and R. G. Griffin, Efficient Dynamic Nuclear Polarization at 800 MHz/527 GHz with Trityl-Nitroxide Biradicals, *Angewandte Chemie International Edition*, 2015, **54**, 11770–11774.
51 F. Mentink-Vigier, G. Mathies, Y. Liu, A.-L. A.-L. L. Barra, M. A. M. A. Caporini, D. Lee, S. Hediger, R. Griffin, G. De Paëpe, R. G. Griffin and G. De Paëpe, Efficient cross-effect dynamic nuclear polarization without depolarization in high-resolution MAS NMR, *Chemical Science*, 2017, **8**, 8150–8163.
52 W. Zhai, A. Lucini Paioni, X. Cai, S. Narasimhan, J. Medeiros-Silva, W. Zhang, A. Rockenbauer, M. Weingarth, Y. Song, M. Baldus and Y. Liu, Postmodification via Thiol-Click Chemistry Yields Hydrophilic Trityl-Nitroxide Biradicals for Biomolecular High-Field Dynamic Nuclear Polarization, *The Journal of Physical Chemistry B*, 2020, **124**, 9047–9060.
53 X. Cai, A. Lucini Paioni, A. Adler, R. Yao, W. Zhang, D. Beriashvili, A. Safeer, A. Gurinov, A. Rockenbauer, Y. Song, M. Baldus and Y. Liu, Highly Efficient Trityl-Nitroxide Biradicals for Biomolecular High-Field Dynamic Nuclear Polarization, *Chemistry – A European Journal*, 2021, **27**, 12758–12762.
54 T. Halbritter, R. Harrabi, S. Paul, J. Van Tol, D. Lee, S. Hediger, S. Th. Sigurdsson, F. Mentink-Vigier and G. De Paëpe, PyrroTriPol: a semi-rigid trityl-nitroxide for high field dynamic nuclear polarization, *Chem. Sci.*, 2023, **14**, 3852–3864.
55 R. Yao, D. Beriashvili, W. Zhang, S. Li, A. Safeer, A. Gurinov, A. Rockenbauer, Y. Yang, Y. Song, M. Baldus and Y. Liu, Highly bioresistant, hydrophilic and rigidly linked trityl-nitroxide biradicals for cellular high-field dynamic nuclear polarization, *Chemical Science*, 2022, **13**, 14157–14164.
56 D. Wisser, G. Karthikeyan, A. Lund, G. Casano, H. Karoui, M. Yulikov, G. Menzildjian, A. C. Pinon, A. Purea, F. Engelke, S. R. Chaudhari, D. Kubicki, A. J. Rossini, I. B. Moroz, D. Gajan, C. Copéret, G. Jeschke, M. Lelli, L. Emsley, A. Lesage and O. Ouari,

Please do not adjust margins

Please do not adjust margins

BDPA-Nitroxide Biradicals Tailored for Efficient Dynamic Nuclear Polarization Enhanced Solid-State NMR at Magnetic Fields up to 21.1 T, *Journal of the American Chemical Society*, 2018, **140**, 13340–13349.

57 P. Berruyer, S. Björgvinsdóttir, A. Bertarello, G. Stevanato, Y. Rao, G. Karthikeyan, G. Casano, O. Ouari, M. Lelli, C. Reiter, F. Engelke and L. Emsley, Dynamic Nuclear Polarization Enhancement of 200 at 21.15 T Enabled by 65 kHz Magic Angle Spinning, *The Journal of Physical Chemistry Letters*, 2020, **11**, 8386–8391.

58 A. Zagdoun, A. J. Rossini, D. Gajan, A. Bourdolle, O. Ouari, M. Rosay, W. E. Maas, P. Tordo, M. Lelli, L. Emsley, A. Lesage and C. Copéret, Non-aqueous solvents for DNP surface enhanced NMR spectroscopy, *Chem. Commun.*, 2012, **48**, 654–656.

59 Y. Matsuki, T. Maly, O. Ouari, H. Karoui, F. Le Moigne, E. Rizzato, S. Lyubenova, J. Herzfeld, T. Prisner, P. Tordo and R. G. Griffin, Dynamic Nuclear Polarization with a Rigid Biradical, *Angew. Chem. Int. Ed.*, 2009, **48**, 4996–5000.

60 D. J. Kubicki, G. Casano, M. Schwarzwälder, S. Abel, C. Sauvée, K. Ganesan, M. Yulikov, A. J. Rossini, G. Jeschke, C. Copéret, A. Lesage, P. Tordo, O. Ouari and L. Emsley, Rational design of dinitroxide biradicals for efficient cross-effect dynamic nuclear polarization, *Chem. Sci.*, 2015, **7**, 550–558.

61 A. Venkatesh, G. Casano, Y. Rao, F. De Biasi, F. A. Perras, D. J. Kubicki, D. Siri, S. Abel, H. Karoui, M. Yulikov, O. Ouari and L. Emsley, Deuterated TEKPol Biradicals and the Spin-Diffusion Barrier in MAS DNP, *Angew Chem Int Ed*, 2023, **62**, e202304844.

62 Y. Matsuki, T. Maly, O. Ouari, H. Karoui, F. Le Moigne, E. Rizzato, S. Lyubenova, J. Herzfeld, T. Prisner, P. Tordo and R. G. Griffin, Dynamic Nuclear Polarization with a Rigid Biradical, *Angewandte Chemie International Edition*, 2009, **48**, 4996–5000.

63 T. Maly, G. T. Debelouchina, V. S. Bajaj, K.-N. Hu, C.-G. Joo, M. L. Mak–Jurkauskas, J. R. Sirigiri, P. C. A. van der Wel, J. Herzfeld, R. J. Temkin and R. G. Griffin, Dynamic nuclear polarization at high magnetic fields, *The Journal of Chemical Physics*, 2008, **128**, 052211.

64 C. Presti, A. S. L. Thankamony, J. G. Alauzun, P. H. Mutin, D. Carnevale, C. Lion, H. Vezin, D. Laurencin and O. Lafon, NMR and EPR Characterization of Functionalized Nanodiamonds, *The Journal of Physical Chemistry C*, 2015, **119**, 12408–12422.

65 H. Nagashima, J. Trébosc, Y. Kon, O. Lafon and J. Amoureux, Efficient transfer of DNP-enhanced ^{1}H magnetization to half-integer quadrupolar nuclei in solids at moderate spinning rate, *Magn Reson Chem*, 2021, **59**, 920–939.

66 M. P. Hanrahan, Y. Chen, R. Blome-Fernández, J. L. Stein, G. F. Pach, M. A. S. Adamson, N. R. Neale, B. M. Cossairt, J. Vela and A. J. Rossini, Probing the Surface Structure of Semiconductor Nanoparticles by DNP SENS with Dielectric Support Materials, *J. Am. Chem. Soc.*, 2019, **141**, 15532–15546.

67 F. A. Perras, U. Chaudhary, I. I. Slowing and M. Pruski, Probing Surface Hydrogen Bonding and Dynamics by Natural Abundance, Multidimensional, ^{17}O DNP-NMR Spectroscopy, *J. Phys. Chem. C*, 2016, **120**, 11535–11544.

68 D. J. Kubicki, A. J. Rossini, A. Purea, A. Zagdoun, O. Ouari, P. Tordo, F. Engelke, A. Lesage and L. Emsley, Amplifying Dynamic Nuclear Polarization of Frozen Solutions by Incorporating Dielectric Particles, *J. Am. Chem. Soc.*, 2014, **136**, 15711–15718.

69 A. Zagdoun, G. Casano, O. Ouari, G. Lapadula, A. J. Rossini, M. Lelli, M. Baffert, D. Gajan, L. Veyre, W. E. Maas, M. Rosay, R. T. Weber, C. Thieuleux, C. Coperet, A. Lesage, P. Tordo and L. Emsley, A Slowly Relaxing Rigid Biradical for Efficient Dynamic Nuclear Polarization Surface-Enhanced NMR Spectroscopy: Expeditious Characterization of Functional Group Manipulation in Hybrid Materials, *J. Am. Chem. Soc.*, 2012, **134**, 2284–2291.

70 T. Sato, Y. Hamada, M. Sumikawa, S. Araki and H. Yamamoto, Solubility of Oxygen in Organic Solvents and Calculation of the Hansen Solubility Parameters of Oxygen, *Ind. Eng. Chem. Res.*, 2014, **53**, 19331–19337.

71 R. Battino, T. R. Rettich and T. Tominaga, The Solubility of Oxygen and Ozone in Liquids, *Journal of Physical and Chemical Reference Data*, 1983, **12**, 163–178.

72 A. Venkatesh, G. Casano, Y. Rao, F. De Biasi, F. A. Perras, D. J. Kubicki, D. Siri, S. Abel, H. Karoui, M. Yulikov, O. Ouari and L. Emsley, Deuterated TEKPol Biradicals and the Spin-Diffusion Barrier in MAS DNP, *Angewandte Chemie International Edition*, **n/a**, e202304844.

73 T. Dubroca, A. N. A. N. Smith, K. J. K. J. Pike, S. Froud, R. Wylde, B. Trociewitz, J. E. McKay, F. Mentink-Vigier, J. van Tol, S. Wi, W. W. Brey, J. R. Long, L. Frydman and S. Hill, A quasi-optical and corrugated waveguide microwave transmission system for simultaneous dynamic nuclear polarization NMR on two separate 14.1 T spectrometers, *Journal of Magnetic Resonance*, 2018, **289**, 35–44.

74 J. van Tol, L.-C. Brunel and R. J. Wylde, A quasioptical transient electron spin resonance spectrometer operating at 120 and 240 GHz, *Review of Scientific Instruments*, 2005, **76**, 074101.

75 F. Neese, The ORCA program system, *Wiley Interdisciplinary Reviews: Computational Molecular Science*, 2012, **2**, 73–78.

76 M. D. Hanwell, D. E. Curtis, D. C. Lonie, T. Vandermeersch, E. Zurek and G. R. Hutchison, Avogadro: An advanced semantic chemical editor, visualization, and analysis platform, *Journal of Cheminformatics*, 2012, **4**, 1–17.

77 S. Grimme, A. Hansen, S. Ehlert and J.-M. Mewes, r 2 SCAN-3c: A “Swiss army knife” composite electronic-structure method, *J. Chem. Phys.*, 2021, **154**, 064103.

78 A. V. Marenich, C. J. Cramer and D. G. Truhlar, Universal Solvation Model Based on Solute Electron Density and on a Continuum Model of the Solvent Defined by the Bulk Dielectric Constant and Atomic Surface Tensions, *The Journal of Physical Chemistry B*, 2009, **113**, 6378–6396.

79 C. Adamo and V. Barone, Toward reliable density functional methods without adjustable parameters: The PBE0 model, *The Journal of Chemical Physics*, 1999, **110**, 6158–6170.

80 F. Weigend and R. Ahlrichs, Balanced basis sets of split valence, triple zeta valence and quadruple zeta valence quality for H to Rn: Design and assessment of accuracy, *Phys. Chem. Chem. Phys.*, 2005, **7**, 3297.

81 A. A. Auer, V. A. Tran, B. Sharma, G. L. Stoychev, D. Marx, F. Neese, A. A. Auer, V. A. Tran, B. Sharma, G. L. Stoychev and A. A. Auer, A case study of density functional theory and domain-based local pair natural orbital coupled cluster for vibrational effects on EPR hyperfine coupling constants : vibrational perturbation theory versus ab initio molecular dynamics constants : vibrational, *Molecular Physics*, 2020, **0**, 1–16.

Please do not adjust margins

Please do not adjust margins

82 E. Caldeweyher, S. Ehlert, A. Hansen, H. Neugebauer, S. Spicher, C. Bannwarth and S. Grimme, A generally applicable atomic-charge dependent London dispersion correction, *The Journal of Chemical Physics*, 2019, **150**, 154122.

83 N. Mardirossian and M. Head-Gordon, *ω* B97M-V: A combinatorially optimized, range-separated hybrid, meta-GGA density functional with VV10 nonlocal correlation, *The Journal of Chemical Physics*, 2016, **144**, 214110.

84 K. Tagami, A. Equbal, I. Kaminker, B. Kirtman and S. Han, Biradical rotamer states tune electron J coupling and MAS dynamic nuclear polarization enhancement, *Solid State Nuclear Magnetic Resonance*, 2019, **101**, 12–20.

85 S. Stoll and R. D. Britt, General and efficient simulation of pulse EPR spectra., *Phys. Chem. Chem. Phys.*, 2009, **11**, 6614–25.

86 P. Eastman, J. Swails, J. D. Chodera, R. T. McGibbon, Y. Zhao, K. A. Beauchamp, L.-P. Wang, A. C. Simmonett, M. P. Harrigan, C. D. Stern, R. P. Wiewiora, B. R. Brooks and V. S. Pande, OpenMM 7: Rapid development of high performance algorithms for molecular dynamics, *PLOS Computational Biology*, 2017, **13**, e1005659.

87 C. Tian, K. Kasavajhala, K. A. A. Belfon, L. Raguette, H. Huang, A. N. Migues, J. Bickel, Y. Wang, J. Pincay, Q. Wu and C. Simmerling, ff19SB: Amino-Acid-Specific Protein Backbone Parameters Trained against Quantum Mechanics Energy Surfaces in Solution, *Journal of Chemical Theory and Computation*, 2020, **16**, 528–552.

88 E. Stendardo, A. Pedone, P. Cimino, M. Cristina Menziani, O. Crescenzi and V. Barone, Extension of the AMBER force-field for the study of large nitroxides in condensed phases: an ab initio parameterization, *Physical Chemistry Chemical Physics*, 2010, **12**, 11697.

89 X. He, V. H. Man, W. Yang, T.-S. Lee and J. Wang, A fast and high-quality charge model for the next generation general AMBER force field, *The Journal of Chemical Physics*, 2020, **153**, 114502.

90 F. Hecker, L. Fries, M. Hiller, M. Chiesa and M. Bennati, 17O Hyperfine Spectroscopy Reveals Hydration Structure of Nitroxide Radicals in Aqueous Solutions, *Angewandte Chemie International Edition*, 2023, **62**, e202213700.

91 T. Lu and F. Chen, Multiwfn: A multifunctional wavefunction analyzer, *Journal of Computational Chemistry*, 2012, **33**, 580–592.

92 H. Sato, V. Kathirvelu, A. Fielding, J. P. Blinco, A. S. Micallef, S. E. Bottle, S. S. Eaton and G. R. Eaton, Impact of molecular size on electron spin relaxation rates of nitroxyl radicals in glassy solvents between 100 and 300 K, *Molecular Physics*, 2007, **105**, 2137–2151.

93 V. Kathirvelu, C. Smith, C. Parks, M. A. Mannan, Y. Miura, K. Takeshita, S. S. Eaton and G. R. Eaton, Relaxation rates for spirocyclohexyl nitroxyl radicals are suitable for interspin distance measurements at temperatures up to about 125 K, *Chem. Commun.*, 2009, 454–456.

94 A. P. Jagtap, M.-A. Geiger, D. Stöppler, M. Orwick-Rydmark, H. Oschkinat and S. Th. Sigurdsson, bcTol: a highly water-soluble biradical for efficient dynamic nuclear polarization of biomolecules, *Chem. Commun.*, 2016, **52**, 7020–7023.

95 I. A. Kirilyuk, Y. F. Polienko, O. A. Krumkacheva, R. K. Strizhakov, Y. V. Gatilov, I. A. Grigor'ev and E. G. Bagryanskaya, Synthesis of 2,5-Bis(spirocyclohexane)-Substituted Nitroxides of Pyrroline and Pyrrolidine Series, Including Thiol-Specific Spin Label: An Analogue of MTSSL with Long Relaxation Time, *J. Org. Chem.*, 2012, **77**, 8016–8027.

96 G. Stevanato, G. Casano, D. J. Kubicki, Y. Rao, L. E. Hofer, G. Menzildjian, H. Karoui, D. Siri, M. Cordova, M. Yulikov, G. Jeschke, M. Lelli, A. Lesage, O. Ouari and L. Emsley, Open and Closed Radicals: Local Geometry around Unpaired Electrons Governs Magic-Angle Spinning Dynamic Nuclear Polarization Performance, *J. Am. Chem. Soc*, 2020, **142**, 33.

97 J. Soetbeer, P. Gast, J. J. Walish, Y. Zhao, C. George, C. Yang, T. M. Swager, R. G. Griffin and G. Mathies, Conformation of bis-nitroxide polarizing agents by multi-frequency EPR spectroscopy, *Physical Chemistry Chemical Physics*, 2018, **20**, 25506–25517.

98 M. A. Geiger, A. P. Jagtap, M. Kaushik, H. Sun, D. Stöppler, S. T. Sigurdsson, B. Corzilius and H. Oschkinat, Efficiency of Water-Soluble Nitroxide Biradicals for Dynamic Nuclear Polarization in Rotating Solids at 9.4 T: bcTol-M and cyolyl-TOTAPOL as New Polarizing Agents, *Chemistry - A European Journal*, 2018, **24**, 13485–13494.

99 S. R. Chaudhari, D. Wisser, A. C. Pinon, P. Berruyer, D. Gajan, P. Tordo, O. Ouari, C. Reiter, F. Engelke, C. Copéret, M. Lelli, A. Lesage and L. Emsley, Dynamic Nuclear Polarization Efficiency Increased by Very Fast Magic Angle Spinning, *J. Am. Chem. Soc.*, 2017, **139**, 10609–10612.

100 P. Negrier, M. Barrio, J. Ll. Tamarit, D. Mondieig, M. J. Zuriaga and S. C. Perez, Conformational Polymorphism: The Missing Phase of 1,1,2,2-Tetrachloroethane (Cl 2 HC–CHCl 2), *Crystal Growth & Design*, 2013, **13**, 2143–2148.

101 M. Wolska-Pietkiewicz, A. Grala, I. Justyniak, D. Hryciuk, M. Jędrzejewska, J. Grzonka, K. J. Kurzydłowski and J. Lewiński, From Well-Defined Alkylzinc Phosphinates to Quantum-Sized ZnO Nanocrystals, *Chemistry – A European Journal*, 2017, **23**, 11856–11865.

102 D. Lee, M. Wolska-Pietkiewicz, S. Badoni, A. Grala, J. Lewiński and G. De Paëpe, Disclosing Interfaces of ZnO Nanocrystals Using Dynamic Nuclear Polarization: Sol-Gel versus Organometallic Approach, *Angew. Chem. Int. Ed.*, 2019, **58**, 17163–17168.

Please do not adjust margins